IEEE Photonics Journal
An IEEE Photonics Society Publication

Open Access

Bottle Beams in Nonlocally Defocusing Nonlinear Media

Volume 11, Number 4, August 2019

Yuanqiang Peng
Yunqi Li
Xiaolin Wu
Weiyi Hong

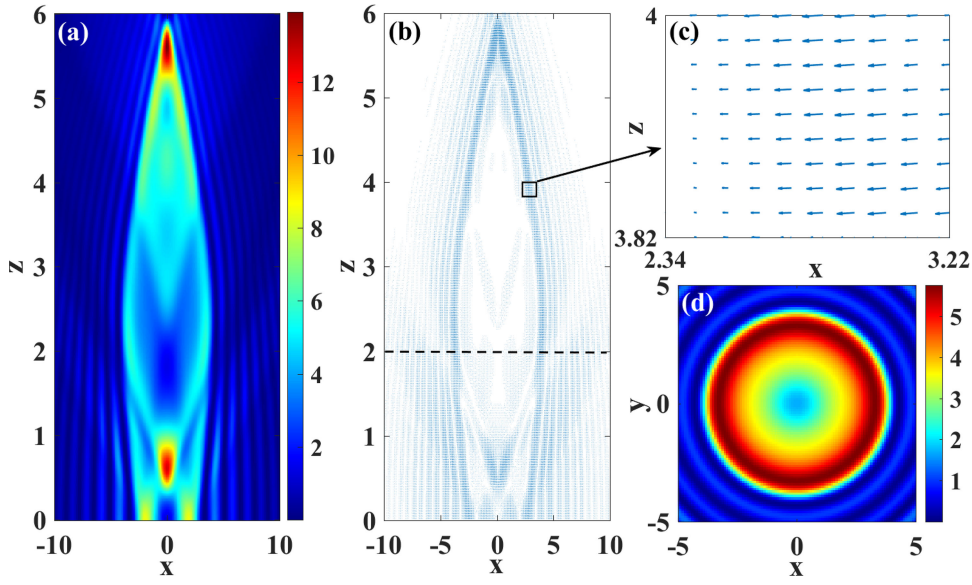

DOI: 10.1109/JPHOT.2019.2933367

Bottle Beams in Nonlocally Defocusing Nonlinear Media

Yuanqiang Peng, Yunqi Li, Xiaolin Wu, and Weiyi Hong

Guangdong Provincial Key Laboratory of Nanophotonic Functional Materials and Devices, South China Normal University, Guangzhou 510631, China

DOI:10.1109/JPHOT.2019.2933367

Manuscript received July 4, 2019; revised July 19, 2019; accepted August 2, 2019. Date of publication August 5, 2019; date of current version August 15, 2019. This work was supported by the National Natural Science Foundation of China under Grant 11874019. Corresponding author: Weiyi Hong (e-mail: hongwy@m.scnu.edu.cn).

Abstract: The dynamics of the inward-focusing ring Airy beam in nonlocally defocusing nonlinear media is investigated in detail, and a bottle beam shape can be observed by adjusting the amplitude of the inward-focusing ring Airy beam and the nonlocality of the media. The gradient force of the bottle beam is numerically studied. It is worth mentioning that the bottle beams are formed in the nonlinear regime, which indicates that much higher intensity is allowable for these beams than those in the linear regime. Our approach and results may pave the way to the optical tweezers in the nonlinear regime.

Index Terms: Ring Airy beam, bottle beam, nonlocally defocusing nonlinear media.

1. Introduction

Airy beam was discovered by G. Siviloglou and realized in the experiment in 2007 [1], [2], which has attracted considerable research interest due to its nondiffracting, self-healing properties, and unique self-bending behavior in the absence of any external potential [1], [3], [4]. With the advancement of research on the novel Airy beam, N. Efremidis proposed another derivative version of the Airy beam calling the ring Airy beam [5]: An Airy beam with circular symmetry, which was later experimentally implemented [6]. Lately, the ring Airy beam has become one of the hottest topics of nonlinear optics due to its abrupt self-focusing property that it can autofocus by following a parabolic trajectory toward its focus, and suddenly increases by orders of magnitude right before its focal point [5]. Abruptly autofocusing property enables the ring Airy beam to have enormously potential applications in creating ablation spots [6], biomedical treatment [7], nonlinear optical processes [8] and optical manipulations [9]–[11].

In the nonlinear optics, the optical Kerr effect (OKE) [12]–[14] is a fundamentally physical phenomenon in the nonlinear interactions of light with materials. The OKE refers to the light-intensity dependence of the refractive index n, that is, $n = n_0 + N$, where n_0 is its linear part and N is the light-induced nonlinear refractive index (NRI). What's more, the self-focusing/defocusing of the OKE refers to the phenomenon that the optical beam propagating in the bulk medium with the homogeneous n_0 can focus or defocus itself by inducing NRI. As the importantly intrinsic properties of the OKE, nonlocality means that the light-induced refractive index change of a material at a particular location is decided by the light intensity in a certain neighborhood of this location [15]. Besides, there are various interesting properties induced by the nonlocality, like the suppression of collapse [16] and the support of vortex/multi-pole solitons [17], [18]. In this paper, we find that the ring Airy

beam propagating in nonlocally defocusing nonlinear media exhibits a hollow bottle shape, which is so-called the bottle beam. Generally, the bottle beam refers to a light field having an apparent low intensity region entirely or partially surrounded by a high-intensity region, which has been first proposed by Arlt and Padgett in 2000 [19]. Ever since, an optical bottle beam has attracted more and more attentions for its unique applications by utilizing gradient optical forces in particle manipulation [20]–[22]. A variety of methods have been proposed for generating the bottle beam, such as diffractive optical elements [9], computer-generated hologram [19], axicon [23], moiré techniques [24], speckle pattern [25] and spatial light modulator [26]. Recently, some researches have been studied a microscale nonparaxial optical bottle beams [27], a dynamic bottle beams [28] and a terahertz bottle beam [29]. In addition, owing to surface plasmon polaritons'(SPP) unique properties, it can simultaneously generate SPP Bessel-like beams and bottle beams [30].

This paper is organized as follows: In Section 2 we describe the theoretical model of the inward-focusing ring Airy beam propagating in nonlocally defocusing nonlinear media, and the generation of a bottle beam by adjusting the parameters of the initial beam and the nonlocality of the media; In Section 3 we further discuss the gradient force field of the bottle beam; In Section 4 we summarize the results of this paper.

2. The Theoretical Model and Numerical Results

The propagation of a light beam in a Kerr medium can be described by the normalized 1 + 2D nonlinear Schrödinger equation [31]–[33]:

$$i\frac{\partial \psi}{\partial \xi}+\frac{1}{2k}\frac{\partial^2 \psi}{\partial \eta_x{}^2}+\frac{1}{2k}\frac{\partial^2 \psi}{\partial \eta_y{}^2}+\frac{kn_2}{n_1}|\psi|^2\psi=0, \tag{1}$$

where $\Psi(\vec{\eta},\xi)$ is the complex amplitude of the optical beam, the variables η_x, η_y, ξ are respectively the transverse and longitudinal coordinates, $k=\omega n_1/c$ is the wave number, n_1 is the refractive index of the media, n_2 is the nonlinear refractive index. By introducing the following scaled quantities for the dimensionless transformation, $z=\xi/kw_0{}^2$, $x=\eta_x/w_0$, $y=\eta_y/w_0$ and $u(x,\ y,z)=kw_0\sqrt{|n_2|/n_1}\Psi(\vec{\eta},\xi)$ with w_0 the characteristic parameter characterizing the beam width, then Eq. (1) becomes:

$$i\frac{\partial u}{\partial z}+\frac{1}{2}\frac{\partial^2 u}{\partial x^2}+\frac{1}{2}\frac{\partial^2 u}{\partial y^2}+\mathrm{sgn}(n_2)|u|^2u=0, \tag{2}$$

We consider a ring Airy beam as the initial condition, which can be expressed in the following form [34]:

$$u(x,y,z=0)=A\cdot Ai\left[\pm\left(r_0-\sqrt{x^2+y^2}\right)\right]\exp\left[\pm a\left(r_0-\sqrt{x^2+y^2}\right)\right], \tag{3}$$

where A is the amplitude of the ring Airy beam [A^2 is the peak intensity normalized by $Ai_m{}^2n_1/(k^2w_0{}^2|n_2|)$ with Ai_m the maximum of the Airy function Ai(*) and calculated to be 0.5357 by normalizing the Airy function], r_0 ($r_0=\sqrt{x_0{}^2+y_0{}^2}$) denotes the radical position of the main ring Airy beam, $\pm$ represent respectively the inward/outward-focusing ring Airy beam, and a is the decaying parameter. In order to simplify, we firstly set $a=0.1$ and $r_0=1$ throughout the whole paper. In the follow, we focus on the propagations of the inward-focusing ring Airy beam (IRAB).

Firstly, we investigate the IRAB propagated in different media by direct numerical integration of Eq. (2) with split-step Fourier transform method (SSFT). More details about the method can be found in [35]. In the simulation, A is set to be 4 to clearly see the different propagation properties among them. It should be noted that the propagation of the IRAB in the self-focusing nonlinear media ($n_2>0$, not shown) would be collapsed due to the 2D local nonlinearity [36]. As reported in Ref. [10], the IRAB exhibits a self-focusing behavior and have one focus in the linear media ($n_2=0$) as shown in Fig. 1(a). For the IRAB propagating in the defocusing nonlinear media ($n_2<0$), it appears a double self-focusing behavior, which forms a bottle beam shape.

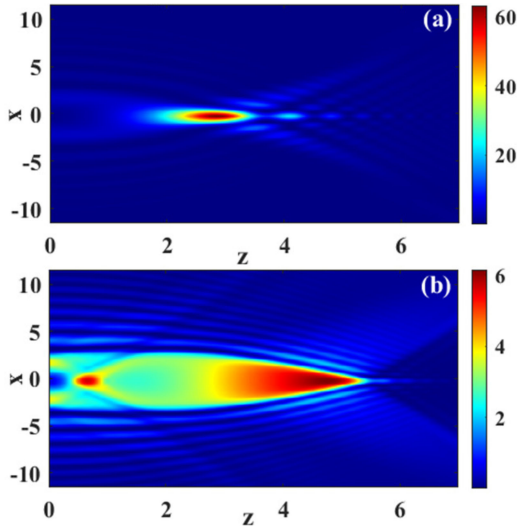

Fig. 1. The evolutions of the IRAB propagating in different media, (a) in the linear media (A = 4), and (b) in the defocusing nonlinear media (A = 4). The 2D figures are cross sections of propagation with y = 0.

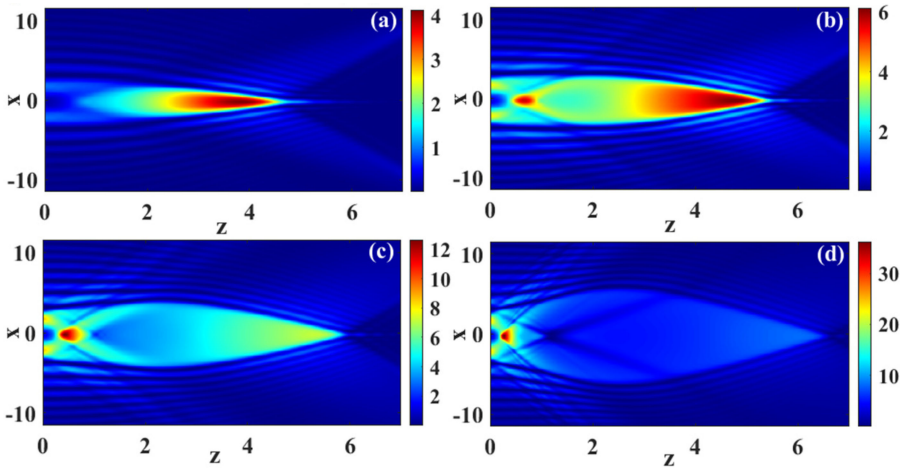

Fig. 2. The evolutions of the IRAB with different amplitude propagating in the defocusing nonlinear media, (a)–(d) correspond to A = 2, A = 4, A = 6, A = 10, respectively. The 2D figures are cross sections of propagation with y = 0.

Furthermore, we show the propagation dynamics of the IRAB in the defocusing nonlinear media as depicted in Fig. 2. For the small amplitude of the IRAB A = 2, the dynamics is very similar to that in the linear media. As the amplitude increases, the double self-focusing during propagation is clearly visible, as shown in Figs. 2(b) and 2(c) for the cases of A = 4 and A = 6, respectively. For the case of A = 6, an interesting phenomenon is observed that the beam propagation exhibits a bottle shape for its light field having an apparently low intensity region entirely or partially surrounded by a high-intensity region. However, for the case of the larger amplitude of A = 10, the propagation of the beam can no longer maintain the bottle shape, but shows surprisingly an “X-type” region, as depicted in Fig. 2(d). In order to see the evolution of the beam intensity during propagation, we plot the intensity at x = 0 and y = 0 as a function of z for the different case of A as depicted in Fig. 3. For the small intensity such as A = 2, it is clearly seen the slow self-focusing during

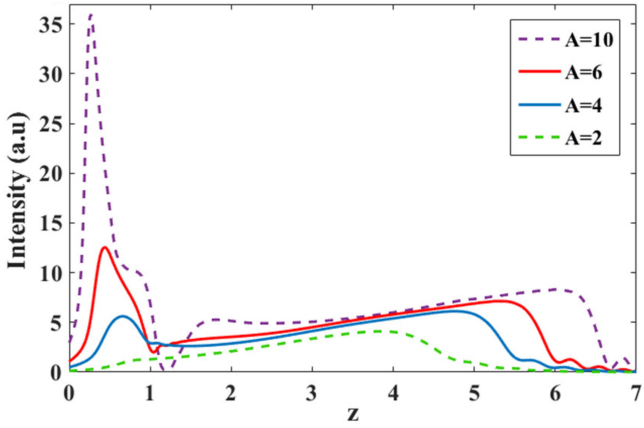

Fig. 3. The evolutions of the IRAB intensity $|u|^2_{max}$ for different amplitude in the defocusing nonlinear media, the purple dash line is A = 10, the red one is A = 6, the blue one is A = 4 and the green dash line is A = 2.

propagation. As the intensity increases, the beam starts to focus rapidly, and the intensity of the first focus increases dramatically with the increasing intensity, then it exhibits a slow self-focusing. It is worth of mentioning that the intensity of the center of the "X-type" region shown in Fig. 2(d) is zero, which indicates that it is benefit for the precise catching of the particles, and this interesting "X-type" region will be further explored in our future work.

In the following, we would like to further explore the effect of the nonlocality on the double self-focusing dynamics discussed above. For the nonlocally nonlinear media, the nonlinear term in Eq. (2) is replaced by a phenomenological model $\delta n(I)$ which reads [37]:

$$\delta n(I) = -\int R\left(\vec{r} - \vec{r'}\right) \cdot \left|u\left(\vec{r'}, z\right)\right|^2 d\vec{r'}, \tag{4}$$

where the negative sign corresponds to a defocusing nonlinearity, $\vec{r}(x, y)$ and z denote the vector spatial and propagative coordinates [37], respectively. $R(\vec{r})$ is the nonlinear nonlocal response function and is chosen to be [18], [38], [39]:

$$R\left(\vec{r} - \vec{r'}\right) = \frac{1}{\pi\sigma^2} \exp\left[-\frac{\left(\vec{r} - \vec{r'}\right)^2}{\sigma^2}\right], \tag{5}$$

with σ the degree of the nonlocality, where $\sigma = 0$ and $\sigma > 0$ denotes respectively the local and nonlocal media [15]. $\delta n(I)$ has been computed by the convolution between the response function and the beam intensity, which is numerically realized by the multiplication between the Fourier transformation of the response function and the beam intensity. Without loss of generality, we respectively consider the weak nonlocality ($\sigma = 0.1$), the medium nonlocality ($\sigma = 0.8$) and the strong nonlocality ($\sigma = 5$, $\sigma = 10$). For the strong nonlocality, the dynamics corresponds to the linear case as shown in Fig. 4(f) [20]. The phenomenon described in Fig. 4(a) is similar to that of the local case. As can be seen from Fig. 4(c), an interesting phenomenon is observed that the bottle beam shape is better defined for the medium nonlocality than that in the local case as depicted in Fig. 2(c), because it is darker in the middle and brighter on the edges. Furthermore, with the help of nonlocality, we have obtained the bottle beam by the IRAB propagating in nonlocally defocusing nonlinear media, and the bottle beam shape is better defined with the degree of the nonlocality between $\sigma = 0.4$ and $\sigma = 1$ as shown in Figs. 4(b)–(d). If we change the amplitude of the IRAB, the nonlocality ($\sigma = 0.8$) will weaken the stability of the bottle beam, as shown in Fig. 5. Figure 5 depicts the propagation dynamics of the IRAB in nonlocally defocusing nonlinear media ($\sigma = 0.8$), and it is clearly seen that the IRAB with the amplitude between A = 4

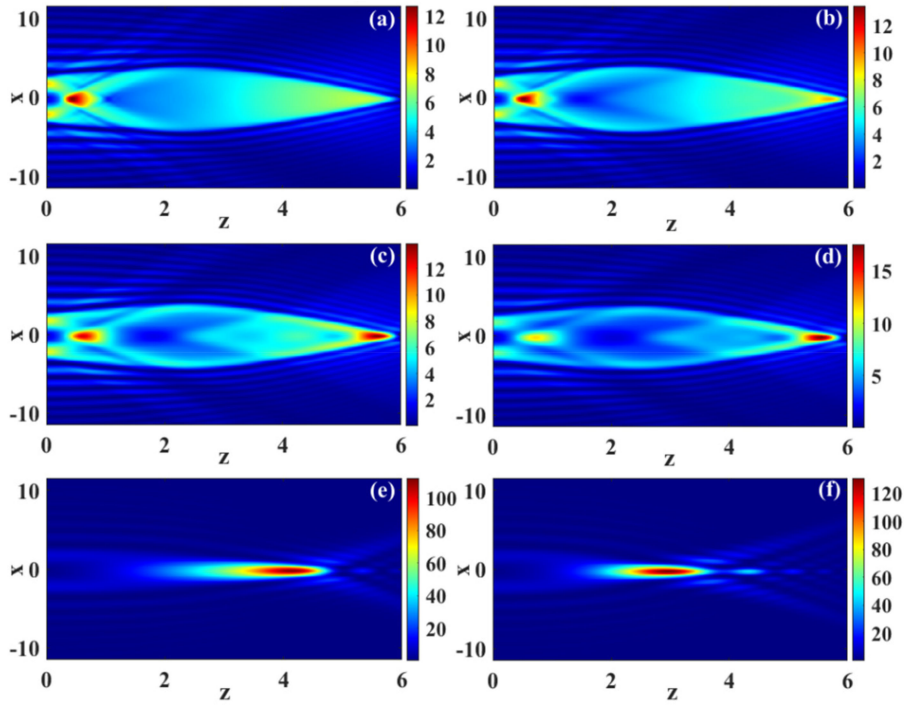

Fig. 4. The evolutions of the IRAB with different nonlocality (σ) propagating in nonlocally defocusing nonlinear media, (a)–(e), (f) correspond to $\sigma = 0.1$, $\sigma = 0.5$, $\sigma = 0.8$, $\sigma = 1$, $\sigma = 5$, $\sigma = 10$, respectively. The initial parameter is A = 6 and the 2D figures are cross sections of propagation with y = 0.

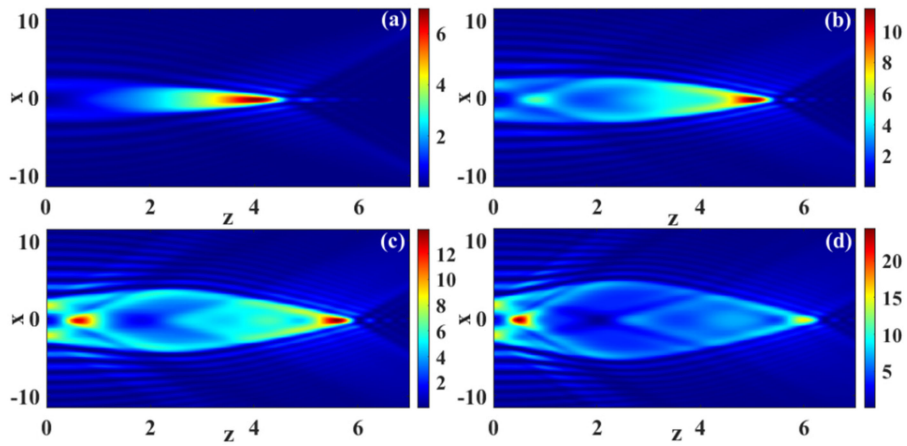

Fig. 5. The evolutions of the IRAB with different amplitude propagating in nonlocally defocusing nonlinear media, (a)–(d) correspond to A = 2, A = 4, A = 6, A = 8, respectively. The 2D figures are cross sections of propagation with y = 0.

and A = 8 is benefit to stabilize the bottle beam shape. Moreover, we also found in Fig. 5(d) the "X-type" region for the sufficient high intensity, which is similar to that in the local case.

In the following, we would like to qualitatively investigate the physical mechanism for the propagation characteristics of the IRAB both in the local and nonlocal nonlinear media discussed above. We show in Fig. 6(a) the distributions of the nonlinear refractive index changes on the x axis at z = 0 for the local and nonlocal cases respectively. The normalized intensity of the beam (on the x axis) is also presented by the dashed curve. For both the local and the nonlocal case, the inner

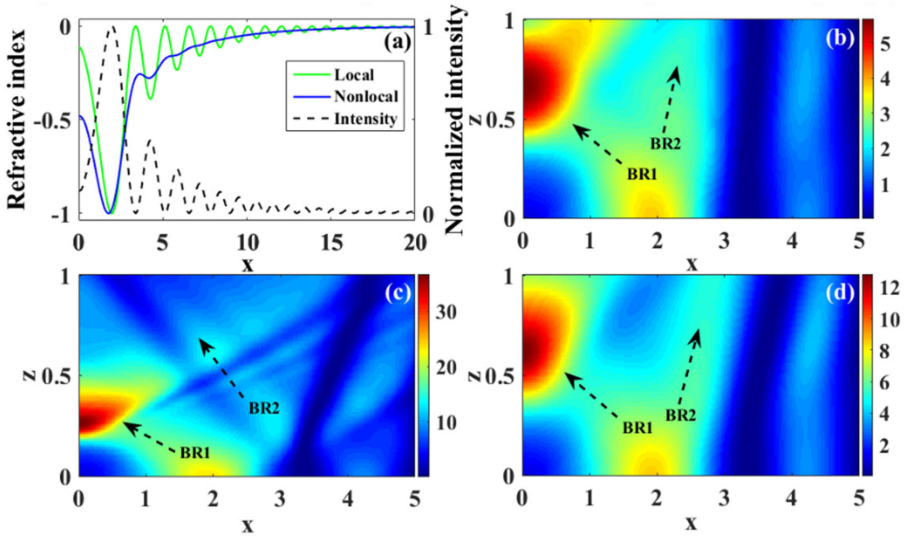

Fig. 6. The figure (a) is the normalized refractive index distributions of the initial input IRAB in locally (the green line)/nonlocally (the blue line) defocusing nonlinear media and the evolutions of normalized intensity $|u|^2_{max}$ of the initial input IRAB (the black dash line). The evolutions of the IRAB propagating in the different media, (b) is in the defocusing nonlinear media (A = 4), (c) is in the defocusing nonlinear media (A = 10) and (d) is in nonlocally defocusing nonlinear media (A = 6, $\sigma = 0.8$).

and outer edges of the main ring samples much higher nonlinear refractive index changes than the central portion, therefore the main ring splits into two rings, as marked by BR1 and BR2 in Figs. 6(b)–(d), which results in double-focusing dynamics discussed above. It is worth noticing that the nonlocality smooths the fluctuation of the nonlinear refractive index change along the radial direction, then BR2 for the nonlocal case shifts faster along the radial direction than that for the local case during propagation, leading to the bottle beam depicted in Fig. 4. For the local case, sufficiently high intensity also totally separates BR1 and BR2, leading to the "X-type" region with zero-intensity in the center as depicted in Fig. 2(d).

To further investigate the relevant properties of bottle beams generated by the IRAB (A = 6, $\sigma = 0.8$), we explore respectively the intensity profiles of bottle beam at transmission distance as shown in Fig. 7. the second row and its corresponding intensity distributions in x-y plane as shown in Fig. 7. the first row. Figure 7 depicts the transverse distributions of the IRAB at different propagation distance: z = 0.6 (the first focus of the bottle beam), z = 2 (the bottle "body" position of the bottle beam) and z = 5.7 (the second focus of the bottle beam), respectively. For the transverse distributions of bottle beam focus, its intensity distributions from the center of circle decreases along the radius in the intensity profile. And for the bottle "body" position of the bottle beam, the IRAB generates a hollow core, which is surrounded by a high-intensity ring (the main the IRAB ring) in Fig. 7(b1). Apart from these, Figure 7(d) depicts the intensity at x = 0 and y = 0 as a function of z with $\sigma = 0.8$ and locality in the defocusing nonlinear media. Distinct from the dynamics of local case, the first focus value is similar with the second one in the nonlocal media (the red line). It is worth mentioning that the bottle beams are formed in the nonlinear regime, which indicates that much higher intensity is allowable for these beams than those for the reported bottle beams in the linear regime [9], [19], [23]–[26].

3. The Gradient Force of the Generated Bottle Beam

In this section, we investigate the gradient force of the bottle beam, which is relative to the particle trapping and manipulation [20]. Assuming that a micro particle with refractive index n_3 is in a stable

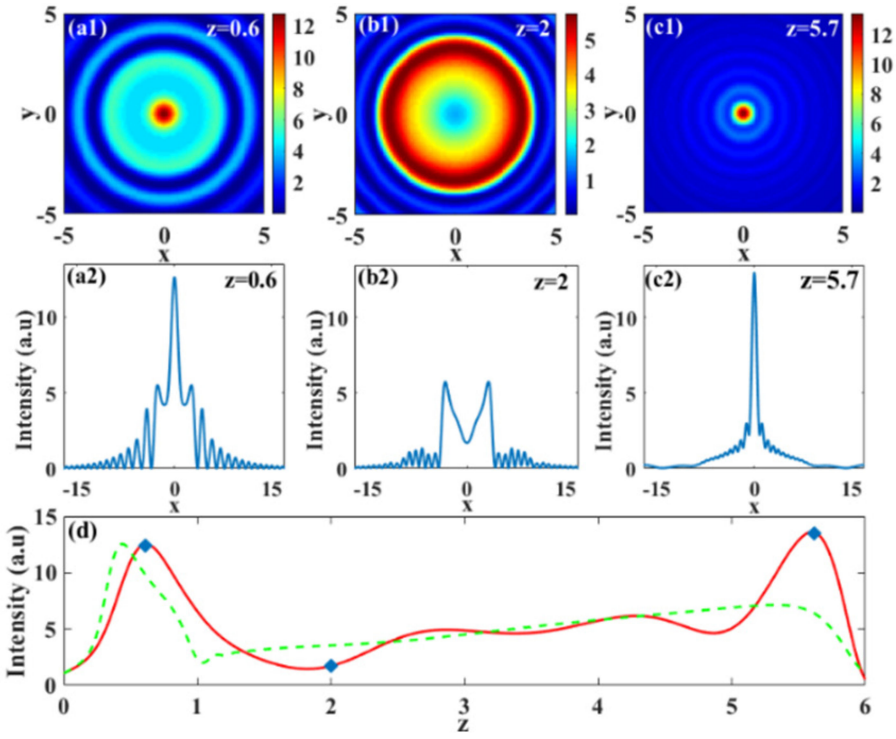

Fig. 7. The first row shows the intensity distributions of the IRAB at different propagation distance (z = 0.6, 2, 5.7) in nonlocally defocusing nonlinear media. The second row is the evolutions of intensity $|u|^2_{max}$ of the IRAB at different propagation distance (z = 0.6, 2, 5.7) in nonlocally defocusing nonlinear media. The third row is the evolutions of the IRAB intensity $|u|^2_{max}$ propagating in nonlocally (the red line)/locally (the green dash line) defocusing nonlinear media, and the blue diamond marks is indicated the different cases of z. The initial parameters are A = 6, $\sigma = 0.8$.

state, the gradient force can be expressed in the following form [40]:

$$\overrightarrow{F}_{grad}(x, y, z) = \frac{2\pi n_4 r^3}{c}\left(\frac{m^2-1}{m^2-2}\right)\nabla I(x, y, z), \tag{6}$$

with n_4 the refractive index of a surrounding medium, r the radius of the micro particle, c the light velocity, $m = n_3/n_4$ the relative refractive index of the particle, $I(x, y, z) = |u(x, y, z)|^2$, respectively. In order to simplify the calculate process of the gradient force, we do not consider the absolute value of the Eq. (6) parameters, only show the numerical gradient force calculation results. Based on the Eq. (6), $I(x, y = 0, z)$ represents the gradient force field distributions in the x-z plane and $I(x, y, z = 2)$ represents the transverse gradient force distributions. In order to achieve a better visualization of the gradient force distributions of the bottle beam, we plot the gradient force intensity $|\vec{F}_{grad}|^2$ distributions of the bottle beam in the x-z plane as depicted in Fig. 8(a), the gradient force field of the bottle beams in the x-z plane and its partial enlargement at the wall of bottle "body" as depicted in Figs. 8(b) and 8(c). As can be seen in the figures, it is clearly seen the gradient force of the inner wall of the bottle beam towards the inside of bottle (attractive force), which indicates that the bottle beam is capable of trapping particles [10], [24], [41]. Furthermore, we plot the transverse gradient force distributions of the bottle beam in nonlocally/locally defocusing nonlinear media at z = 2, y = 0 as a function of x. From Figs. 7(b1) and 8(d), it is clearly seen that there is one considerable gradient force ring corresponding to the inner wall of bottle "body". After exploring the transverse distributions of the gradient force, we find that the maxima of the gradient force are located at the outer edge of the bottle beam as shown in Fig. 8(d), which allows for the particle trapping and manipulation. Distinct from the dynamics of local case, the gradient force on a particle is stronger

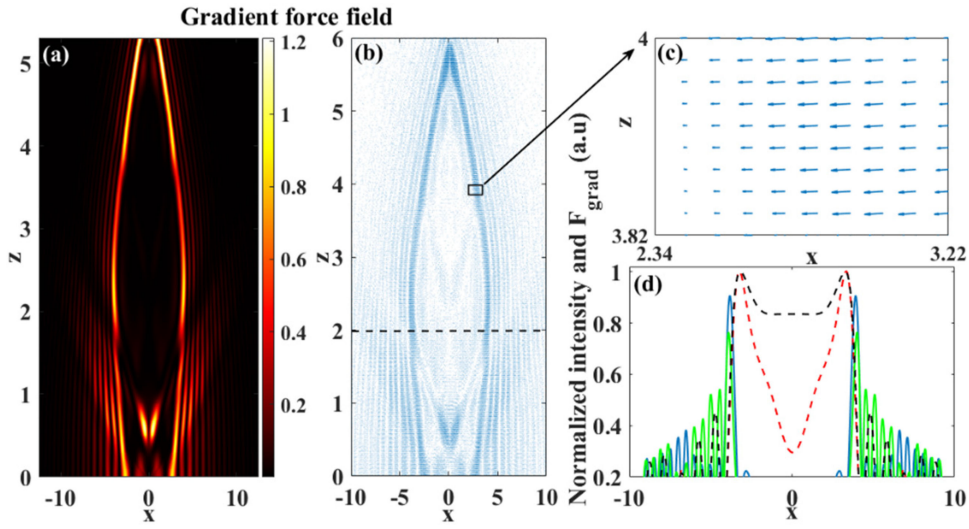

Fig. 8. (a) is the gradient force intensity $|\vec{F}_{grad}|^2$ distributions of the bottle beams, (b) is the gradient force field of the bottle beams (quiver), (c) is the zoom (the black rectangle in Fig. 7(b)) of the bottle beams gradient force field (quiver), (d) is the gradient force of the bottle beam in nonlocally (the blue line)/locally (the green line) defocusing nonlinear media and the normalized intensity distributions of the bottle beam in nonlocally (the red dash line)/locally (the black dash line) defocusing nonlinear media at propagation distance z = 2. The initial parameters are A = 6, $\sigma = 0.8$.

in nonlocally defocusing nonlinear media as depicted in Fig. 8(d). More importantly, the contrast for the nonlocal case is much higher than that for the local case, both for the force and the intensity distribution.

4. Conclusion

In conclusion, the propagation of the IRAB in the defocusing nonlinear media is investigated with split-step Fourier transform method (SSFT) in detail. An interesting phenomenon is observed that the dynamic of the IRAB in the defocusing nonlinear media is a double self-focusing behavior. By adjusting the amplitude of the IRAB and the nonlocality of the media, a bottle beam shape can be observed, and its characteristics are discussed in detail. After calculating the gradient force of the bottle beam, we find that there is a considerable gradient force ring on the inner wall of the bottle beam, which benefits for the particle trapping and manipulation. What's more, we qualitatively investigate the physical mechanism for the propagation characteristics of the IRAB both in the local and nonlocal nonlinear media discussed above. It is worth mentioning that the bottle beams are formed in the nonlinear regime, which indicates that much higher intensity is allowable for these beams than those for the reported bottle beams in the linear regime. Our approach and results may pave the way to the optical tweezers in the nonlinear regime.

References

[1] G. A. Siviloglou and D. N. Christodoulides, "Accelerating finite energy airy beams," *Opt. Lett.*, vol. 32, no. 8, pp. 979–981, 2007.
[2] J. Broky, G. A. Siviloglou, A. Dogariu, and D. N. Christodoulides, "Observation of accelerating airy beams," *Phys. Rev. Lett.*, vol. 99, no. 21, 2007, Art. no. 213901.
[3] J. Broky, G. A. Siviloglou, A. Dogariu, and D. N. Christodoulides, "Self-healing properties of optical airy beams," *Opt. Exp.*, vol. 16, no. 17, pp. 12880–12891, 2008.
[4] G. A. Siviloglou, J. Broky, A. Dogariu, and D. N. Christodoulides, "Ballistic dynamics of airy beams," *Opt. Lett.*, vol. 33, no. 3, pp. 207–209, 2008.
[5] N. K. Efremidis and D. N. Christodoulides, "Abruptly autofocusing waves," *Opt. Lett.*, vol. 35, no. 23, pp. 4045–4047, 2010.

[6] D. G. Papazoglou, N. K. Efremidis, D. N. Christodoulides, and S. Tzortzakis, "Observation of abruptly autofocusing waves," *Opt. Lett.*, vol. 36, no. 10, pp. 1842–1844, 2011.
[7] R. Dasgupta, S. Ahlawat, R. S. Verma, and P. K. Gupta, "Optical orientation and rotation of trapped red blood cells with Laguerre-Gaussian mode," *Opt. Exp.*, vol. 19, no. 8, pp. 7680–7688, 2011.
[8] P. Panagiotopoulos, D. G. Papazoglou, A. Couairon, and S. Tzortzakis, "Sharply autofocused ring-airy beams transforming into non-linear intense light bullets," *Nature Commun.*, vol. 4, 2013, Art. no. 2622.
[9] J. Baumgartl, M. Mazilu, and K. Dholakia, "Optically mediated particle clearing using airy wavepackets," *Nature Photon.*, vol. 2, no. 11, pp. 675–678, 2008.
[10] P. Zhang *et al.*, "Trapping and guiding microparticles with morphing autofocusing airy beams," *Opt. Lett.*, vol. 36, no. 15, pp. 2883–2885, 2011.
[11] M. Manousidaki, D. G. Papazoglou, M. Farsari, and S. Tzortzakis, "Abruptly autofocusing beams enable advanced multiscale photo-polymerization," *Optica*, vol. 3, no. 5, pp. 525–530, 2016.
[12] F. Deng and W. Y. Hong, "Chirp-induced channel of an airy pulse in an optical fiber close to its zero-dispersion point," *IEEE Photon. J.*, vol. 8, no. 6, Dec. 2016, Art. no. 7102807.
[13] F. Deng, W. Y. Hong, and D. M. Deng, "Airy-type solitary wave in highly noninstantaneous Kerr media," *Opt. Exp.*, vol. 24, no. 14, pp. 15997–16002, 2016.
[14] W. Y. Hong, Q. Guo, and L. Li, "Dynamics of optical pulses in highly noninstantaneous Kerr media," *Phys. Rev. A*, vol. 92, no. 2, 2015, Art. no. 023803.
[15] W. Krolikowski *et al.*, "Modulational instability, solitons and beam propagation in spatially nonlocal nonlinear media," *J. Opt. B: Quantum Semiclass. Opt.*, vol. 6, pp. S288–S294, 2004.
[16] O. Bang, W. Krolikowski, J. Wyller, and J. J. Rasmussen, "Collapse arrest and soliton stabilization in nonlocal nonlinear media," *Phys. Rev. E*, vol. 66, no. 4, 2002, Art. no. 046619.
[17] A. I. Yakimenko, V. M. Lashkin, and O. O. Prikhodko, "Dynamics of two-dimensional coherent structures in nonlocal nonlinear media," *Phys. Rev. E*, vol. 73, no. 6, 2006, Art. no. 066605.
[18] D. Buccoliero, A. S. Desyatnikov, W. Krolikowski, and Y. S. Kivshar, "Laguerre and Hermite soliton clusters in nonlocal nonlinear media," *Phys. Rev. Lett.*, vol. 98, no. 5, 2007, Art. no. 053901.
[19] J. Arlt and M. J. Padgett, "Generation of a beam with a dark focus surrounded by regions of higher intensity: The optical bottle beam," *Opt. Lett.*, vol. 25, no. 4, pp. 191–193, 2000.
[20] L. Isenhower, W. Williams, A. Dally, and M. Saffman, "Atom trapping in an interferometrically generated bottle beam trap," *Opt. Lett.*, vol. 34, no. 8, pp. 1159–1161, 2009.
[21] K. Dholakia, P. Reece, and M. Gu, "Optical micromanipulation," *Chem. Soc. Rev.*, vol. 37, no. 1, pp. 42–55, 2008.
[22] D. G. Grier, "A revolution in optical manipulation," *Nature*, vol. 424, no. 6950, pp. 810–816, 2003.
[23] T. J. Du, T. Wang, and F. T. Wu, "Generation of three-dimensional optical bottle beams via focused non-diffracting Bessel beam using an axicon," *Opt. Commun.*, vol. 317, pp. 24–28, 2014.
[24] P. Zhang *et al.*, "Trapping and transporting aerosols with a single optical bottle beam generated by moiré techniques," *Opt. Lett.*, vol. 36, no. 8, pp. 1491–1493, 2011.
[25] V. G. Shvedov, A. V. Rode, Y. V. Izdebskaya, A. S. Desyatnikov, W. Krolikowski, and Y. S. Kivshar, "Selective trapping of multiple particles by volume speckle field," *Opt. Exp.*, vol. 18, no. 3, pp. 3137–3142, 2010.
[26] Z. Zhang, D. Cannan, J. J. Liu, P. Zhang, D. N. Christodoulides, and Z. G. Chen, "Observation of trapping and transporting air-borne absorbing particles with a single optical beam," *Opt. Exp.*, vol. 20, no. 15, pp. 16212–16217, 2012.
[27] R.-S. Penciu *et al.*, "Observation of microscale nonparaxial optical bottle beams," *Opt. Lett.*, vol. 43, no. 16, pp. 3878–3881, 2018.
[28] K. Szulzycki, V. Savaryn, and I. Grulkowski, "Generation of dynamic Bessel beams and dynamic bottle beams using acousto-optic effect," *Opt. Exp.*, vol. 24, no. 21, pp. 23977–23991, 2016.
[29] H. T. Li *et al.*, "Vector measurement and performance tuning of a terahertz bottle beam," *Sci. Rep.*, vol. 8, 2018, Art. no. 13177.
[30] P. Z. Qiu *et al.*, "Polarization controllable device for simultaneous generation of surface plasmon polariton Bessel-like beams and bottle beams," *Nanomaterials*, vol. 8, 2018, Art. no. 975.
[31] Y. R. Shen, *Principles of Nonlinear Optics*. New York, NY, USA: Wiley, 1984, pp. 286–331, chs. 16 and 17.
[32] R. W. Boyd, *Nonlinear Optics*, 3rd ed. Amsterdam, The Netherlands: Academic, 2008, pp. 207–275, chs. 4 and 5.
[33] B. Chen *et al.*, "Evolution of the ring airy Gaussian beams with a spiral phase in the Kerr medium," *J. Opt.*, vol. 18, 2016, Art. no. 055504.
[34] Y. F. Jiang, K. K. Huang, and X. H. Lu, "Propagation dynamics of abruptly autofocusing airy beams with optical vortices," *Opt. Exp.*, vol. 20, no. 17, pp. 18579–18584, 2012.
[35] G. P. Agrawal, *Nonlinear Fiber Optics*, 5th ed. Amsterdam, The Netherlands: Elsevier, 2015.
[36] P. Panagiotopoulos *et al.*, "Nonlinear propagation dynamics of finite-energy airy beams," *Phys. Rev. A*, vol. 86, no. 1, 2012, Art. no. 013842.
[37] W. Krolikowski and O. Bang, "Solitons in nonlocal nonlinear media: Exact results," *Phys. Rev. E*, vol. 63, no. 2, 2001, Art. no. 016610.
[38] M. Shen, W. Li, and R.-K. Lee, "Control on the anomalous interactions of Airy beams in nematic liquid crystals," *Opt. Exp.*, vol. 24, no. 8, pp. 8501–8511, 2016.
[39] M. Shen, J. S. Gao, and L. J. Ge, "Solitons shedding from airy beams and bound states of breathing airy solitons in nonlocal nonlinear media," *Sci. Rep.*, vol. 5, 2015, Art. no. 9814.
[40] Y. Harada and T. Asakura, "Radiation forces on a dielectric sphere in the Rayleigh scattering regime," *Opt. Commun.*, vol. 124, no. 5/6, pp. 529–541, 1996.
[41] V. G. Shvedov, A. S. Desyatnikov, A. V. Rode, W. Krolikowski, and Y. S. Kivshar, "Optical guiding of absorbing nanoclusters in air," *Opt. Exp.*, vol. 17, no. 7, pp. 5743–5757, 2009.